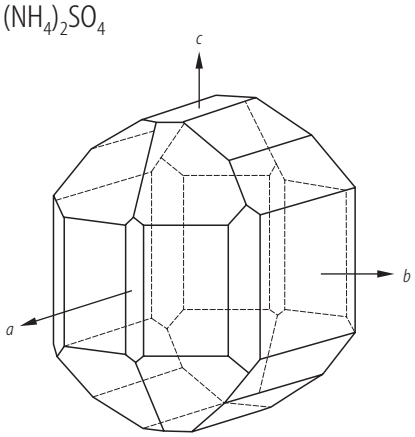

Fig. 39A-1-001. $(NH_4)_2SO_4$. Crystal form with the setting $b > a > c$ [08Gro].

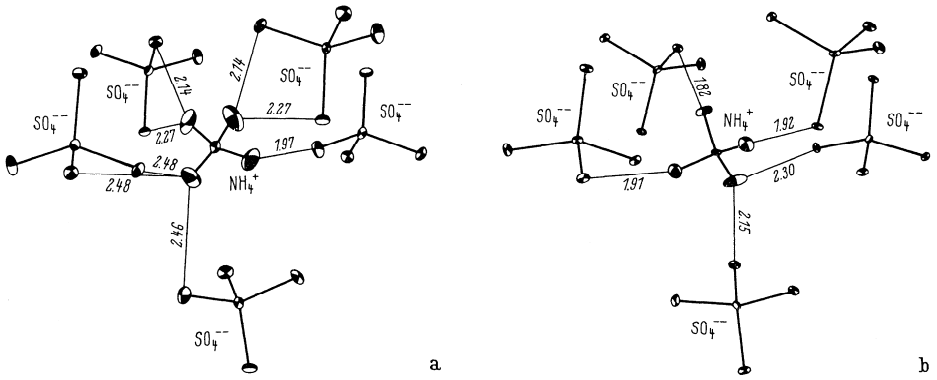

Fig. 39A-1-002. $(NH_4)_2SO_4$. Structures of phases I and II [66Sch]. Neutron diffraction. The environment of $(NH_4)^+$(I). (**a**) RT, (**b**) about 180 K. Atomic distances in [Å].

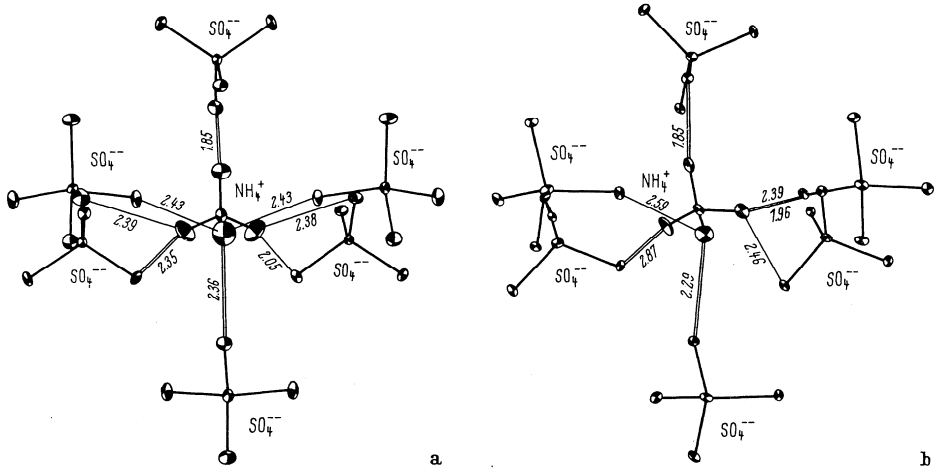

Fig. 39A-1-003. $(NH_4)_2SO_4$. Structures of phases I and II [66Sch]. Neutron diffraction. The environment of $(NH_4)^+$(II). (**a**) RT, (**b**) about 180 K. Atomic distances in [Å].

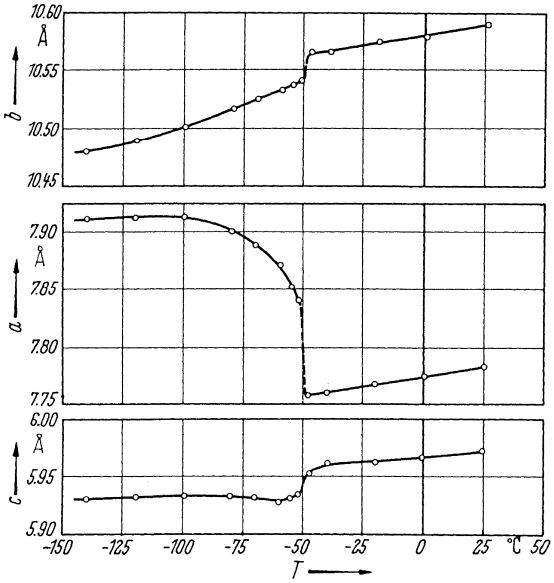

Fig. 39A-1-004. $(NH_4)_2SO_4$. *a*, *b*, *c* vs. *T* [58Hos].

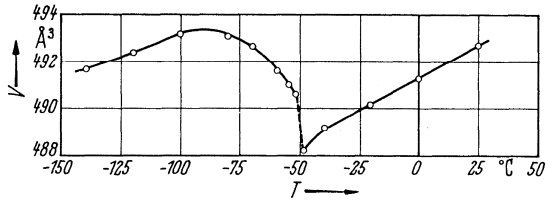

Fig. 39A-1-005. $(NH_4)_2SO_4$. *V* vs. *T* [58Hos]. *V*: volume of the unit cell.

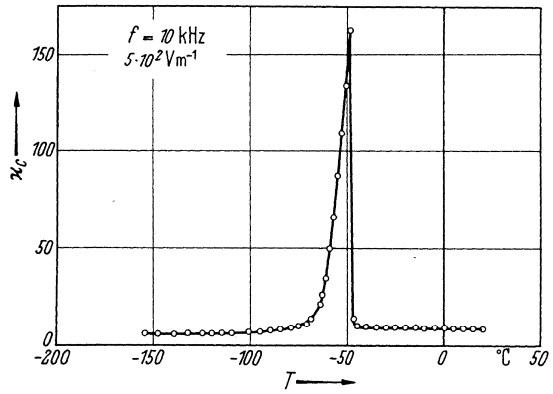

Fig. 39A-1-006. $(NH_4)_2SO_4$. κ_c vs. *T* [58Hos].

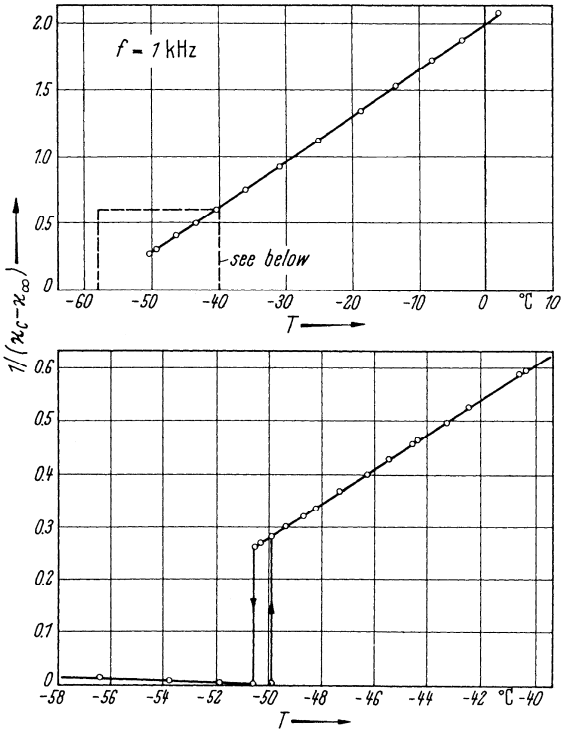

Fig. 39A-1-007. $(NH_4)_2SO_4$. $1/(\kappa_c - \kappa_\infty)$ vs. T [65Unr]. $\kappa_\infty = 9.4(2)$.

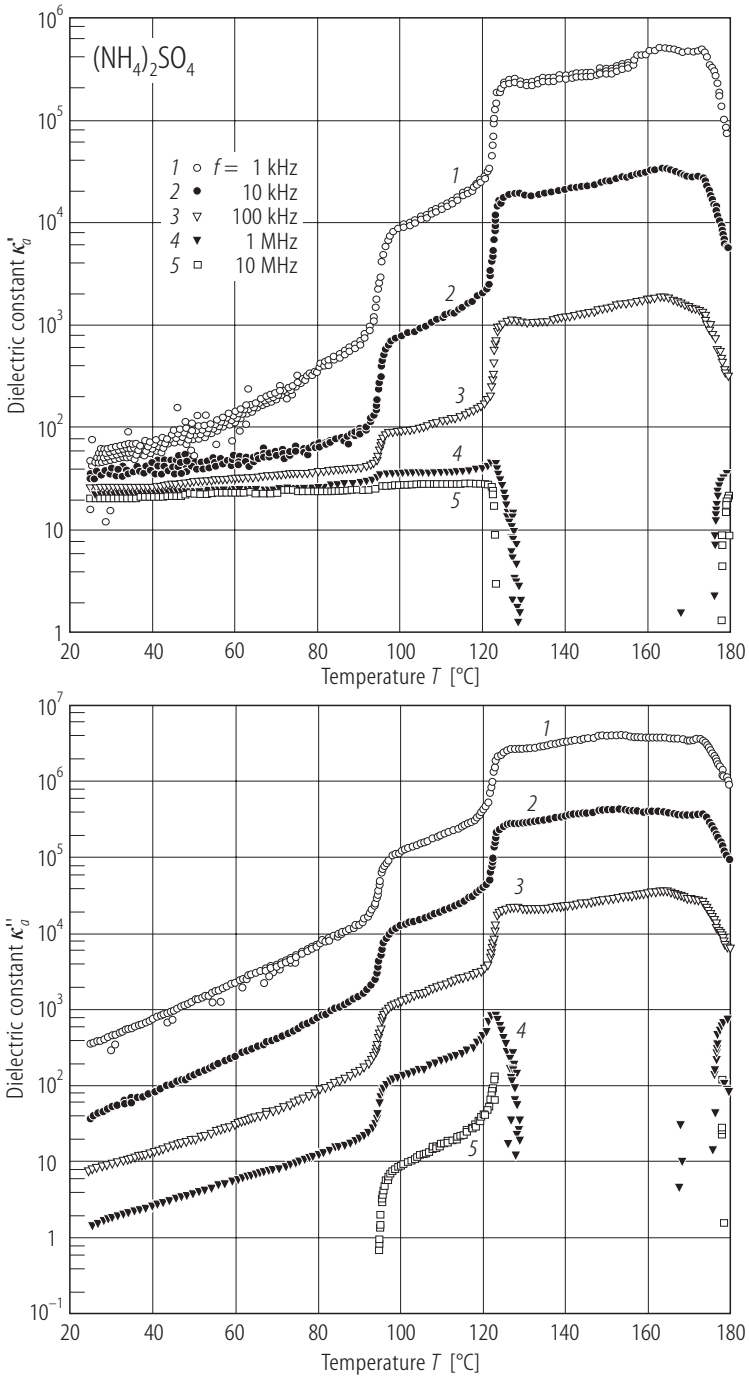

Fig. 39A-1-008. $(NH_4)_2SO_4$. κ_a', κ_a'' vs. T [96Kim2]. Parameter: f. On cooling.

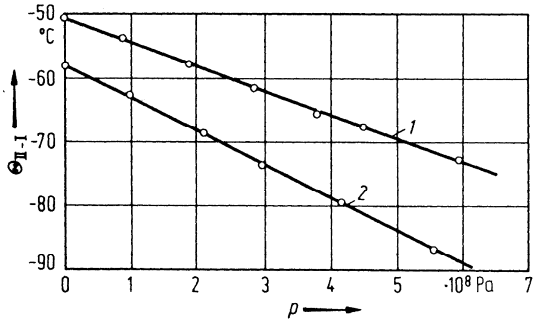

Fig. 39A-1-009. $(NH_4)_2SO_4$, $[(NH_4)_2SO_4]_{0.9}[NH_4BeF_3]_{0.1}$. Θ_{II-I} vs. p [72Pol]. Curve *1*: for $(NH_4)_2SO_4$, *2*: for the solid solution.

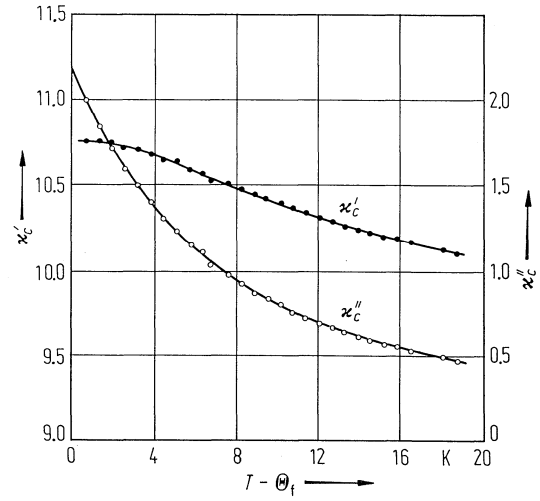

Fig. 39A-1-010. $(NH_4)_2SO_4$. κ_c', κ_c'' vs. $T-\Theta_f$ [80Lut]. $f = 2.3 \cdot 10^{10}$ Hz.

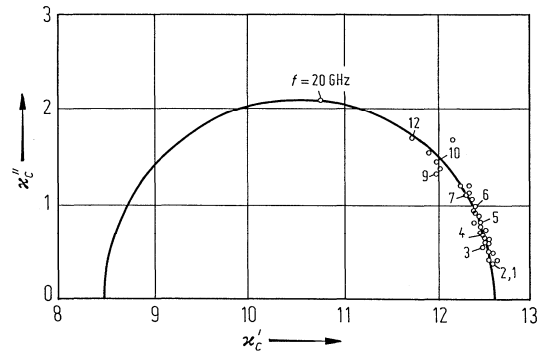

Fig. 39A-1-011. $(NH_4)_2SO_4$. Cole-Cole plot of the complex dielectric constant in the paraelectric phase [79Lut]. $T = -50.482$ °C, 0.42 °C above Θ_f.

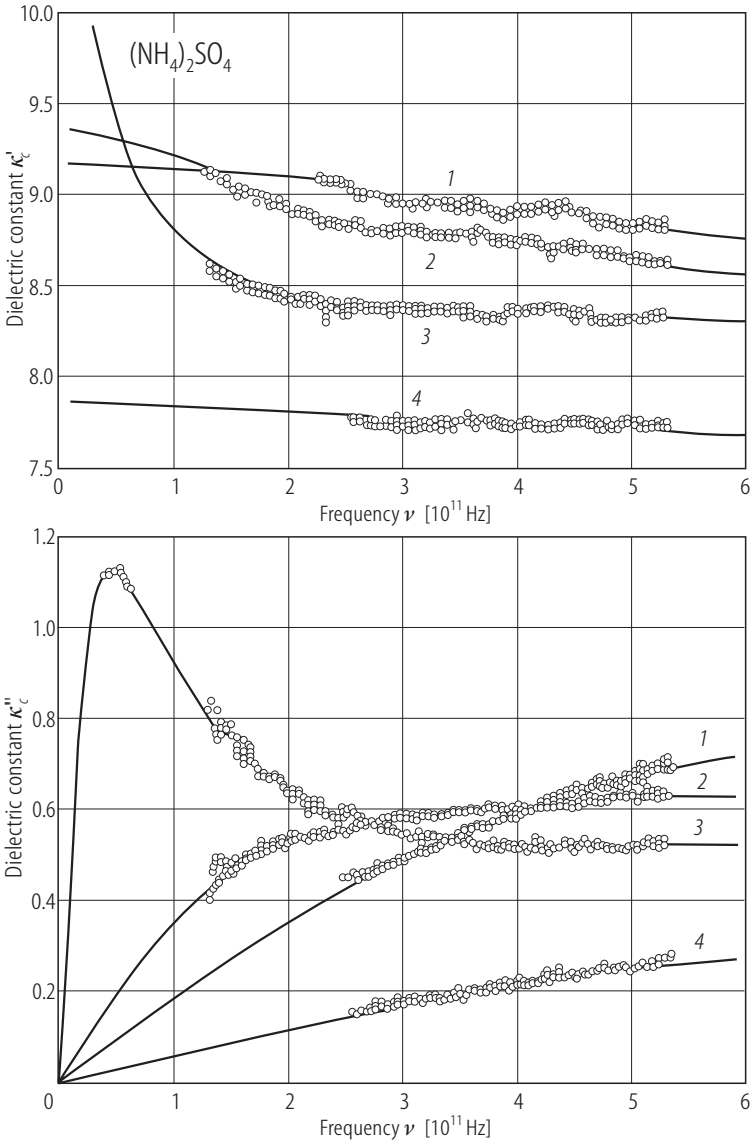

Fig. 39A-1-012. $(NH_4)_2SO_4$. κ_c', κ_c'' vs. ν [88Vol]. Parameter: *T*. Curve *1*: *T* = 376 K, *2*: 297 K, *3*: 225 K, *4*: 196 K.

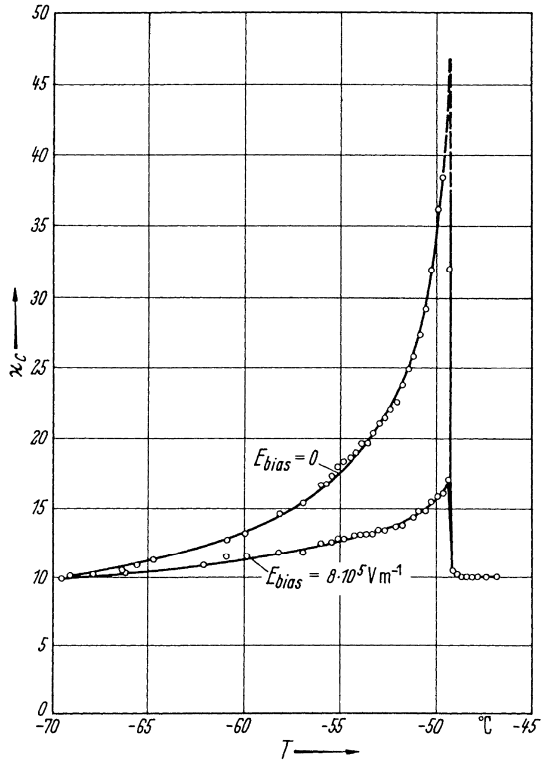

Fig. 39A-1-013. $(NH_4)_2SO_4$. κ_c vs. T [58Hos]. f = 10 kHz. Parameter: E_{bias}.

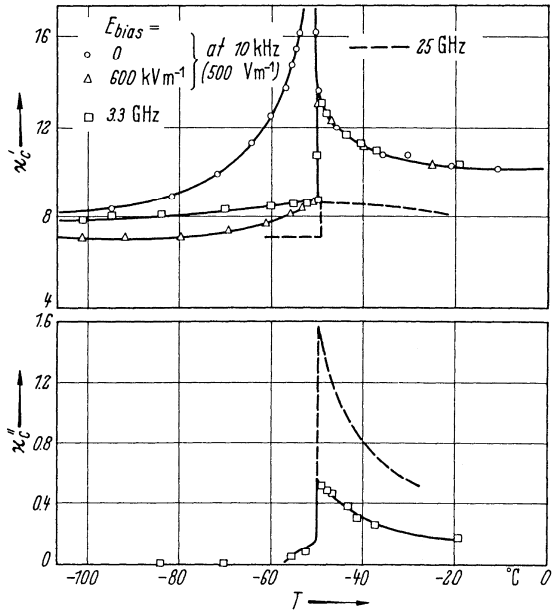

Fig. 39A-1-014. $(NH_4)_2SO_4$. κ_c', κ_c'' vs. T [66Ohs]. Dashed curve: [56Cou].

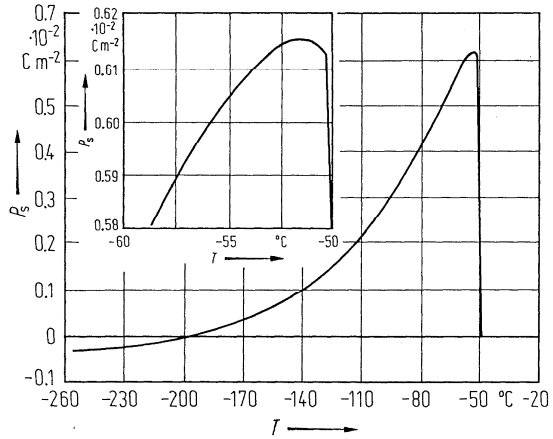

Fig. 39A-1-015. $(NH_4)_2SO_4$. P_s vs. T [70Unr].

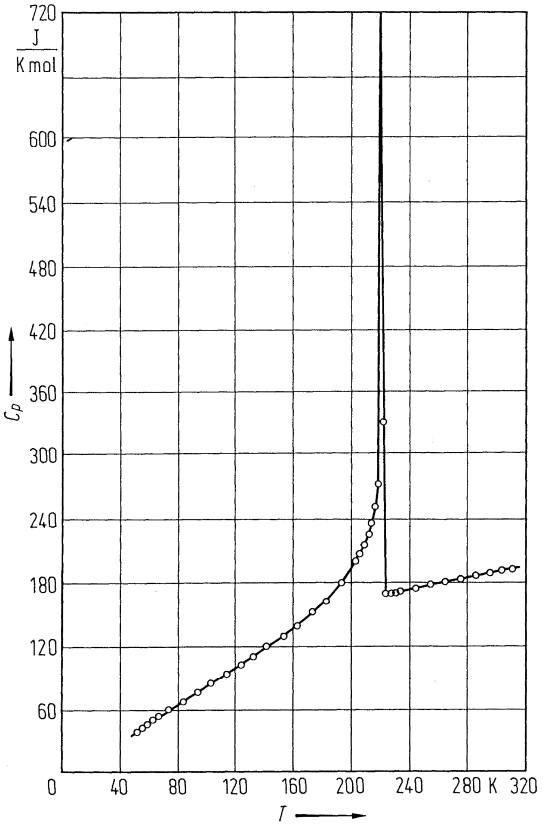

Fig. 39A-1-016. $(NH_4)_2SO_4$. C_p vs. T [45Sho]. C_p: molar heat capacity at constant pressure.

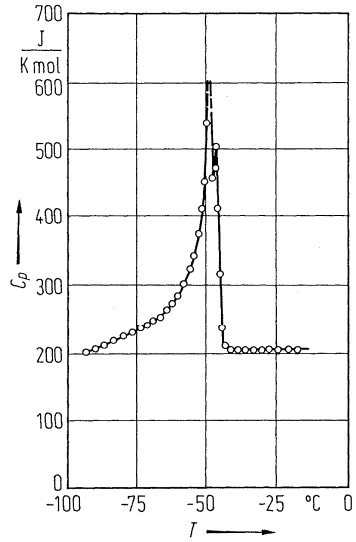

Fig. 39A-1-017. $(ND_4)_2SO_4$. C_p vs. T [58Hos]. C_p: molar heat capacity at constant pressure.

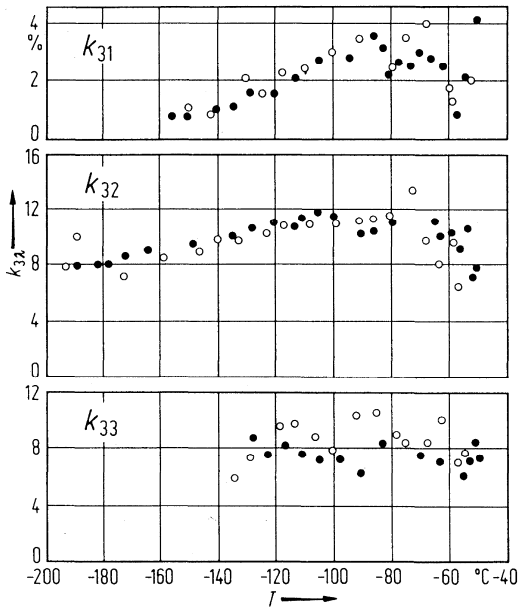

Fig. 39A-1-018. $(NH_4)_2SO_4$. $k_{3\lambda}$ vs. T [73Ike]. $k_{3\lambda}$: electromechanical coupling coefficient. Open circles: on cooling, full circles: on heating.

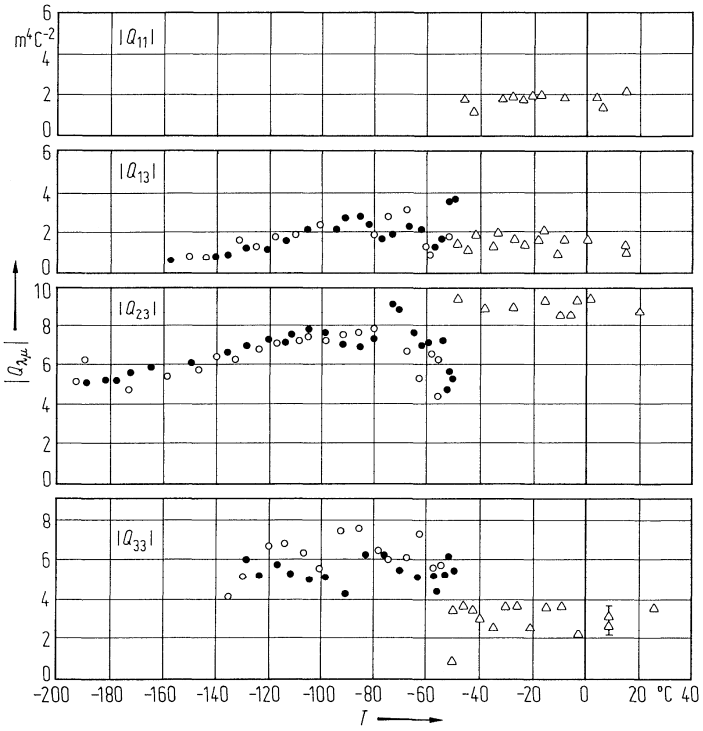

Fig. 39A-1-019. $(NH_4)_2SO_4$. $|Q_{\lambda\mu}|$ vs. T [73Ike, 75Zai]. $Q_{\lambda\mu}$: electrostrictive constant. Values below Θ_{II-I} are obtained from piezoelectric constants assuming that P_s is independent of temperature and should be corrected by taking account of the decrease of P_s at lower temperatures [73Ike]. Open circles: on cooling, full circles: on heating. The triangles above Θ_{II-I} are determined by the measurement of electrostrictive strains at low frequencies [75Zai].

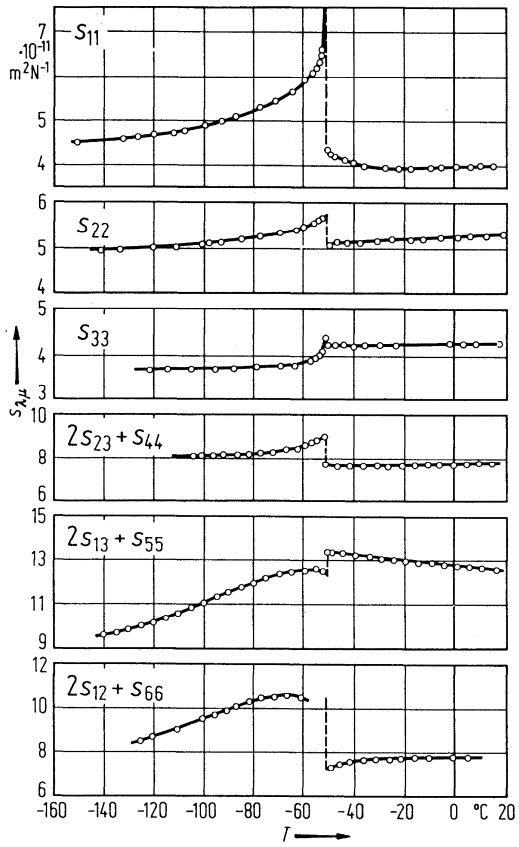

Fig. 39A-1-020. $(NH_4)_2SO_4$. $s_{\lambda\mu}$ vs. T [73Ike]. $s_{\lambda\mu}$: elastic compliance.

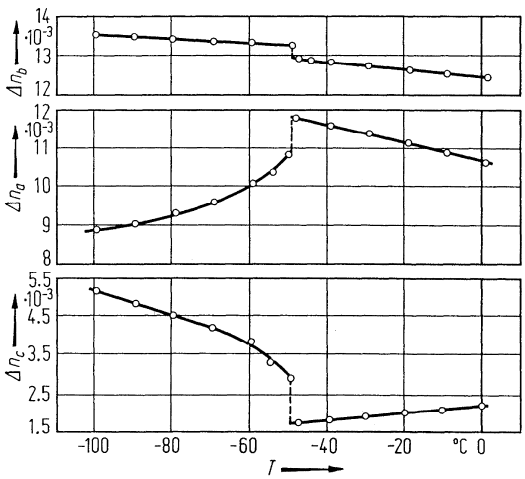

Fig. 39A-1-021. $(NH_4)_2SO_4$. Δn_a, Δn_b, Δn_c vs. T [70Ani]. $\Delta n_a = |\, n_b - n_c \,|$, $\Delta n_b = |\, n_c - n_a \,|$, $\Delta n_c = |\, n_a - n_b \,|$.

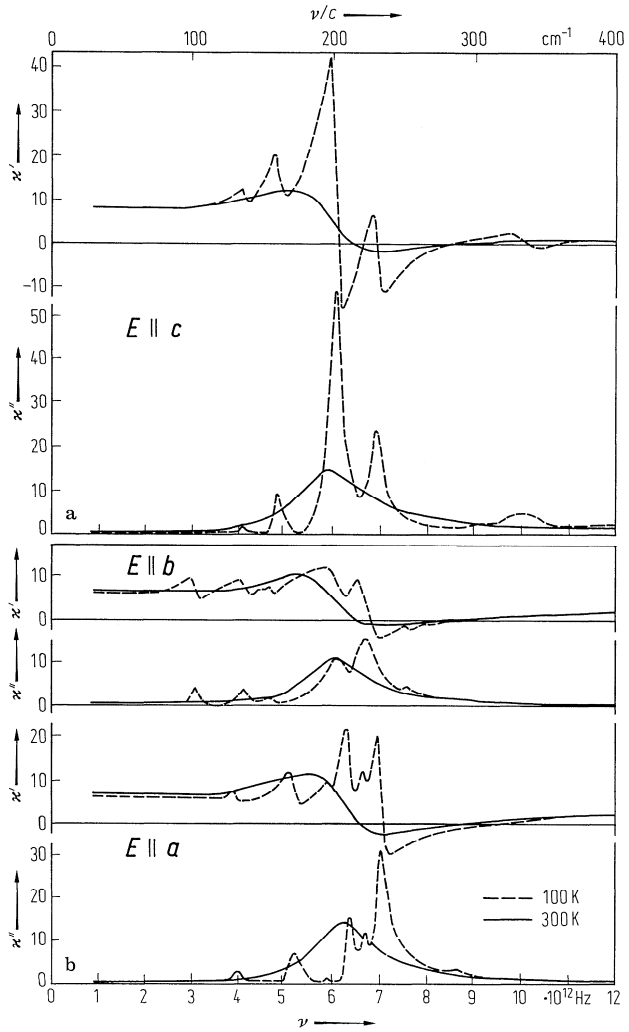

Fig. 39A-1-022. $(NH_4)_2SO_4$. κ', κ'' vs. ν [74Pet]. ν: frequency of incident far-infrared radiation. Polarization of the radiation is parallel to the *c* axis in (**a**), and parallel to the *b* and the *c* axis in (**b**). κ', κ'' are obtained from the reflectivity spectra using Kramers-Kronig analysis.

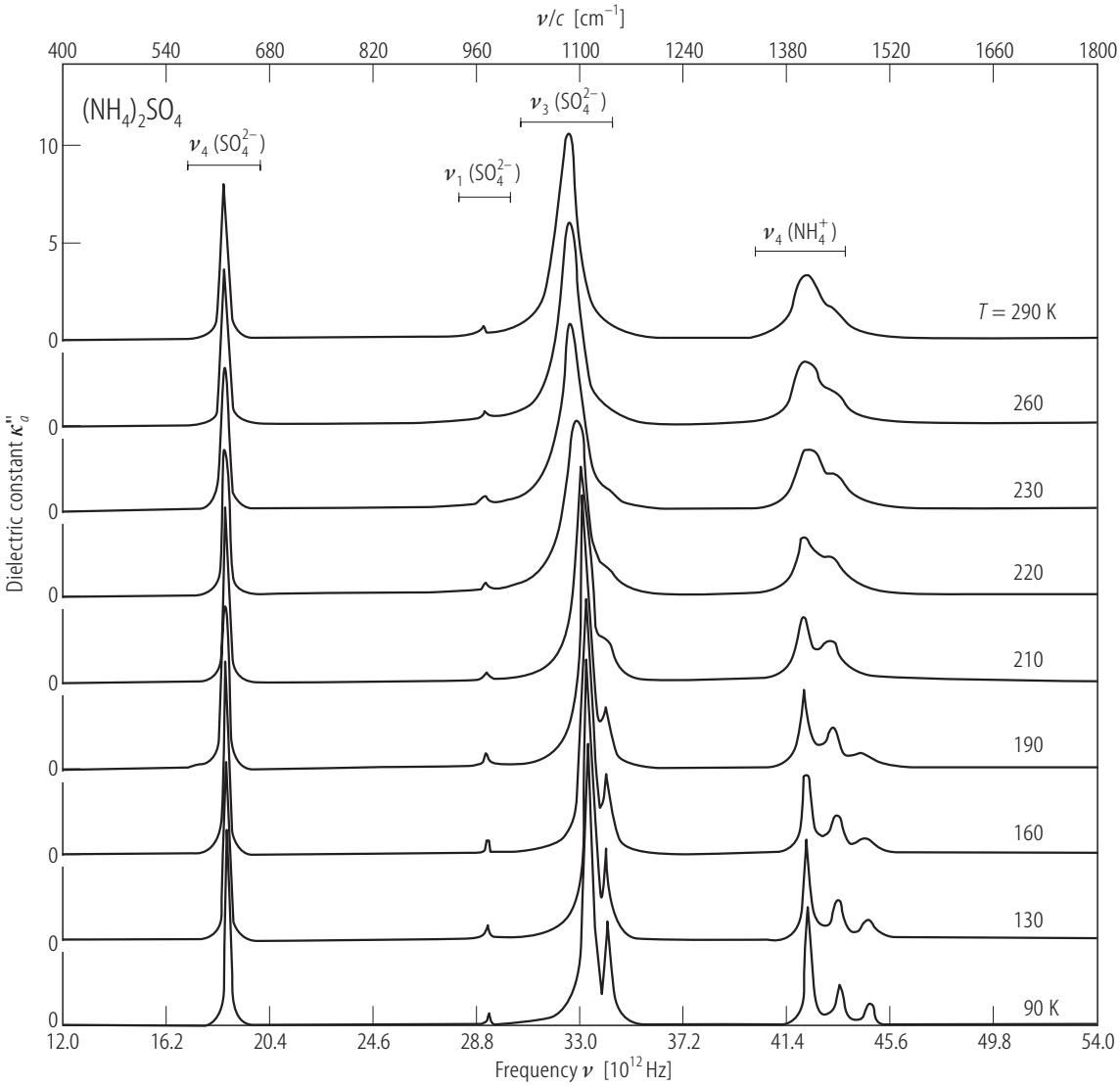

Fig. 39A-1-023. $(NH_4)_2SO_4$. κ_a'' vs. ν [95DeS]. ν: frequency of incident far-infrared radiation. Parameter: T. κ_a'' is obtained from the reflectivity data by the fit of the factorized form of κ.

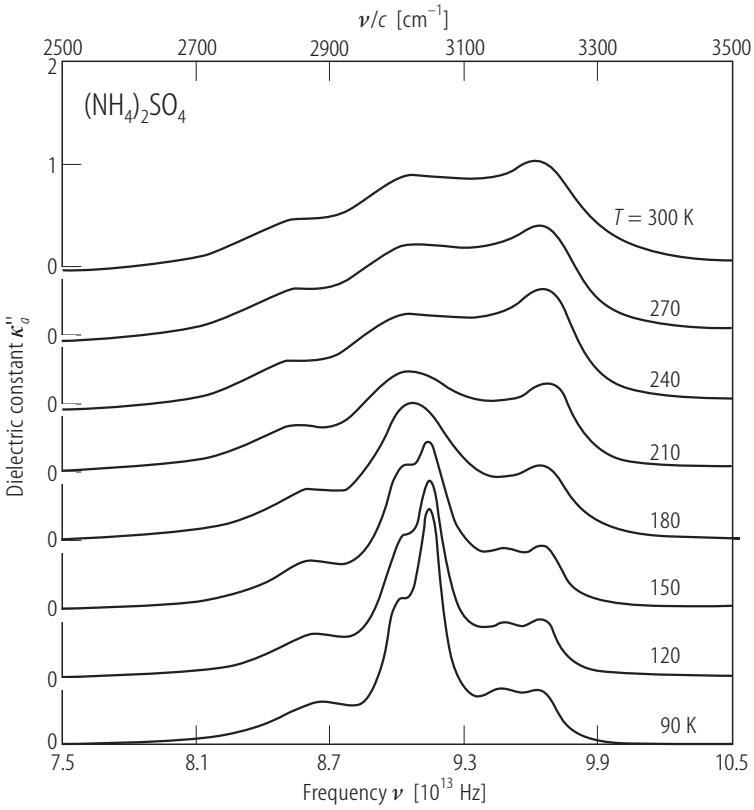

Fig. 39A-1-024. $(NH_4)_2SO_4$. κ_a'' vs. ν [95DeS]. ν: frequency of incident far-infrared radiation. Parameter: T. κ_a'' is obtained from the reflectivity data by the fit of the factorized form of κ.

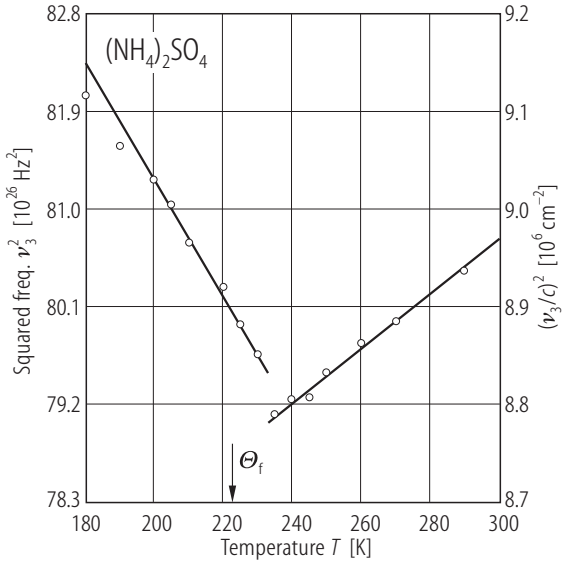

Fig. 39A-1-025. $(NH_4)_2SO_4$. ν_3^2 vs. T [95DeS]. ν_3: frequency of the internal ν_3 mode of NH_4^+ near 3000 cm^{-1}.

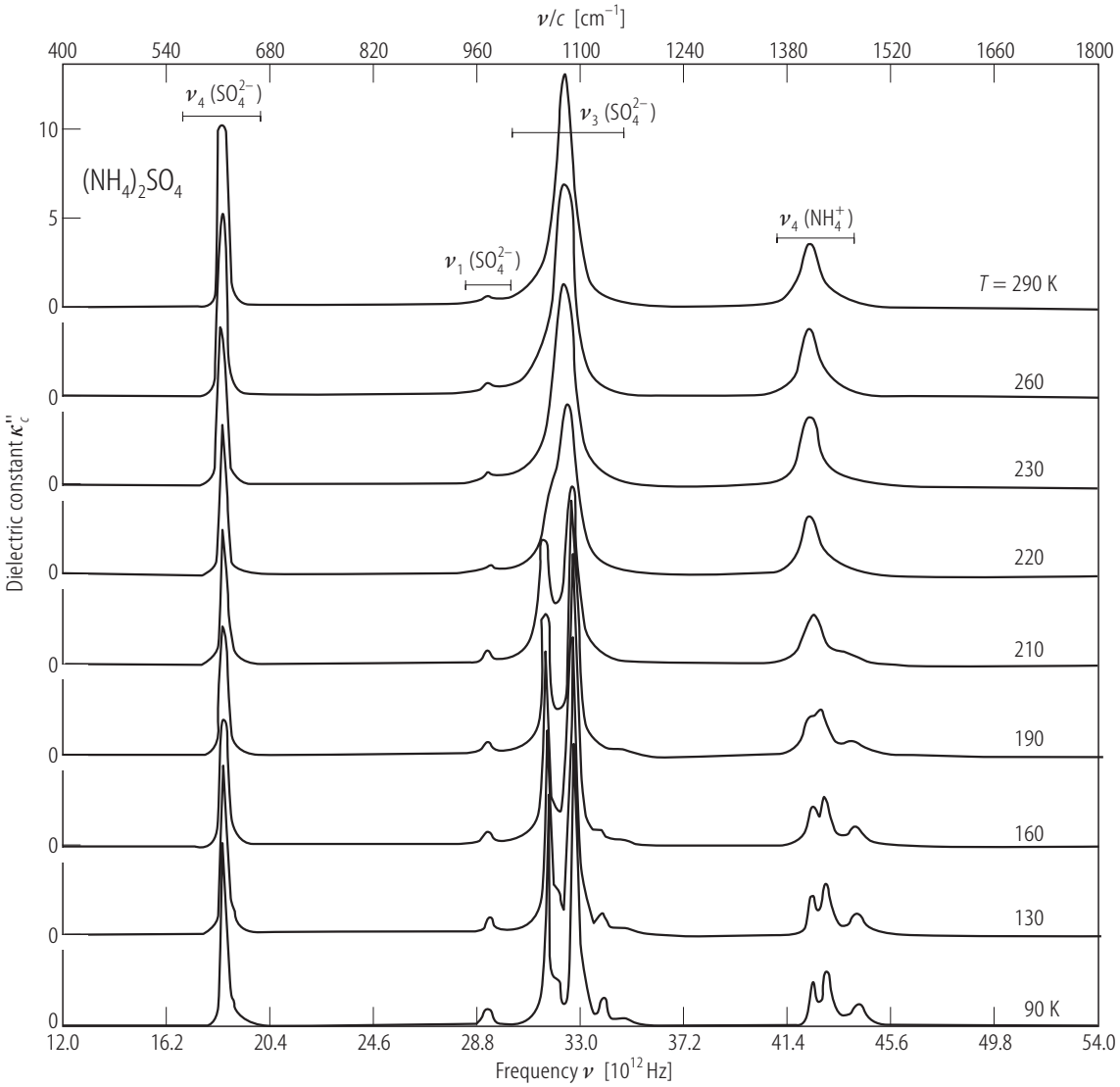

Fig. 39A-1-026. $(NH_4)_2SO_4$. κ_c'' vs. ν [95DeS]. ν: frequency of incident far-infrared radiation. κ_c'' is obtained from the reflectivity data by the fit of the factorized form of κ.

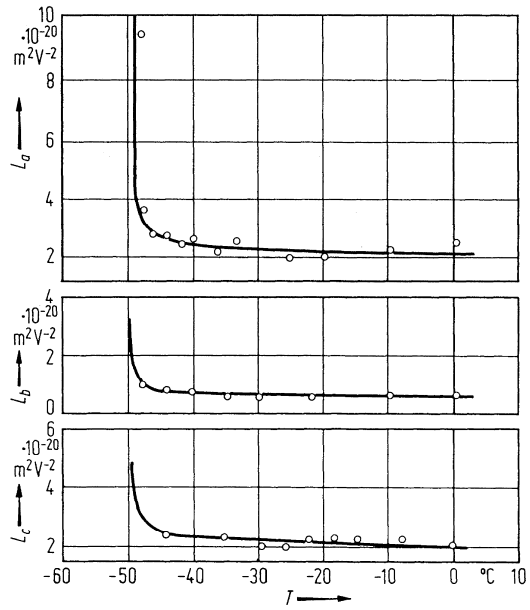

Fig. 39A-1-027. $(NH_4)_2SO_4$. L_a, L_b, L_c vs. T [70Ani]. $L_a = n_c^3 L_{33} - n_b^3 L_{23}$, $L_b = n_a^3 L_{13} - n_c^3 L_{33}$, $L_c = n_b^3 L_{23} - n_a^3 L_{13}$. $L_{\lambda\mu}$: quadratic electrooptic constant for E.

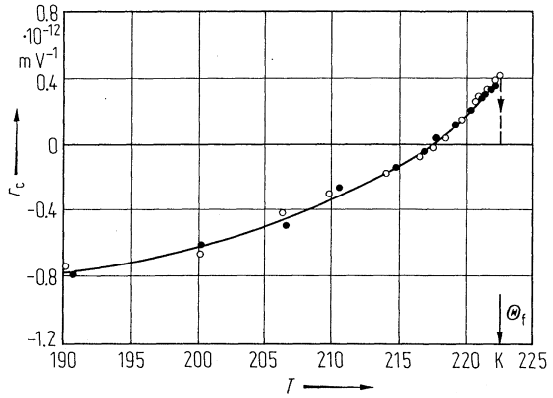

Fig. 39A-1-028. $(NH_4)_2SO_4$. r_c vs. T [76Fou]. $r_c = r_{13} - r_{23}$.

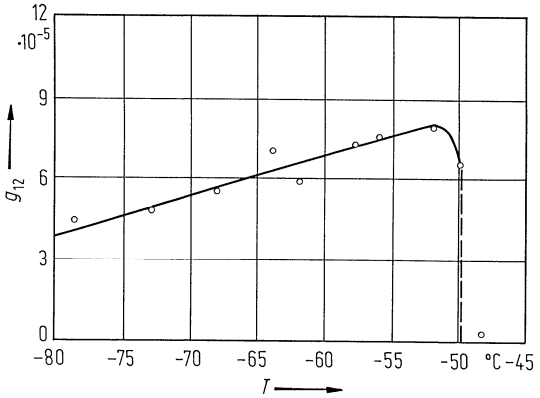

Fig. 39A-1-029. $(NH_4)_2SO_4$. g_{12} vs. T [80Kob]. g_{12}: gyration tensor component. $\lambda = 456.5$ nm.

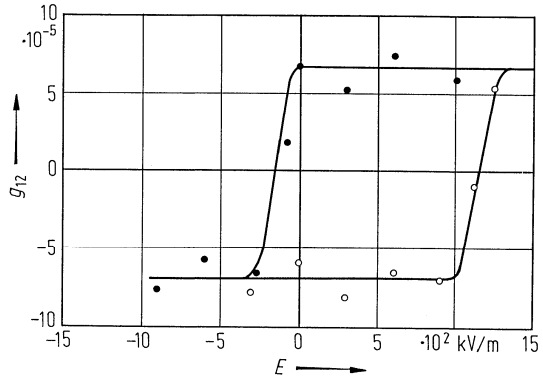

Fig. 39A-1-030. $(NH_4)_2SO_4$. g_{12} vs. E [80Kob]. g_{12}: gyration tensor component. $T = -57$ °C. $\lambda = 456.5$ nm.

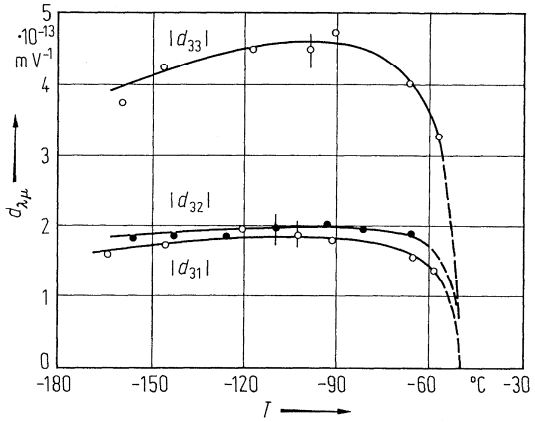

Fig. 39A-1-031. $(NH_4)_2SO_4$. $d_{\lambda\mu}$ vs. T [77Suz]. $d_{\lambda\mu}$: nonlinear optical susceptibility.

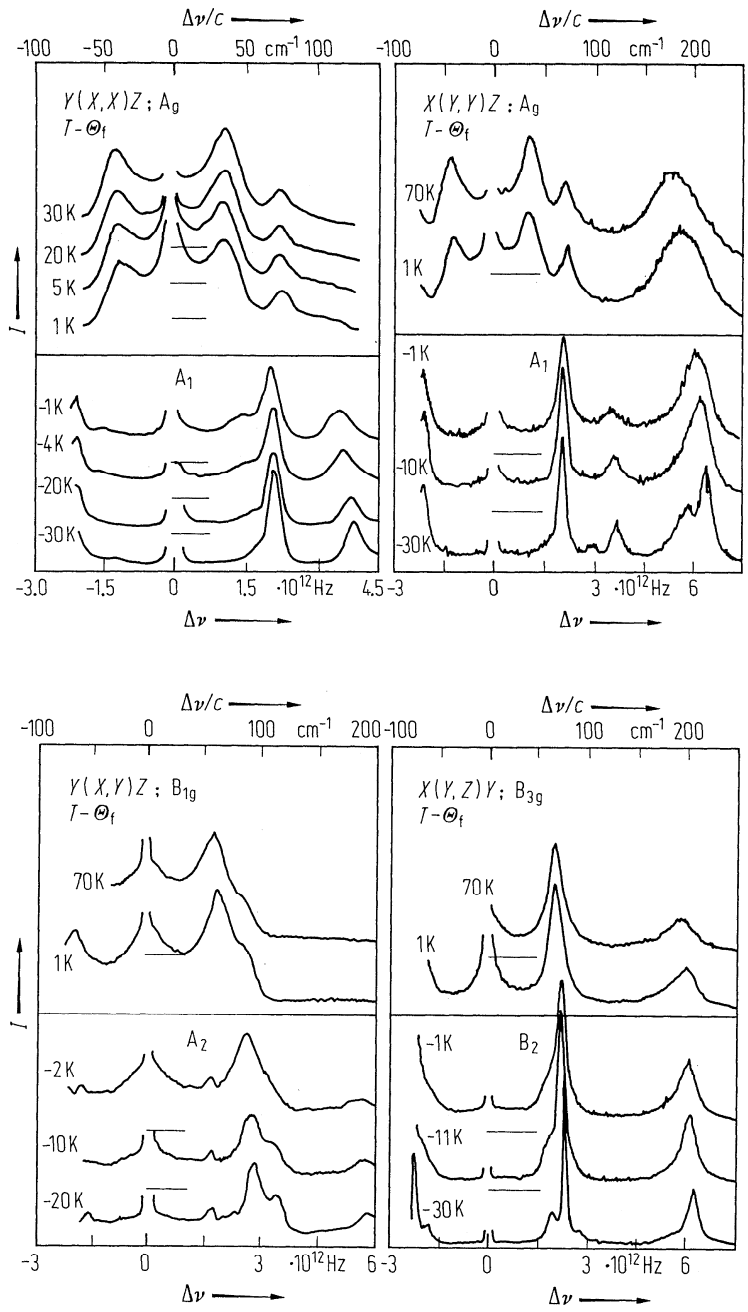

Fig. 39A-1-032. $(NH_4)_2SO_4$. I vs. $\Delta\nu$ above and below Θ_f in the low frequency region [78Unr]. I: Raman scattering intensity, $\Delta\nu$: frequency shift of Raman scattering. Scattering geometries and the corresponding symmetries of phonons are given in the figure.

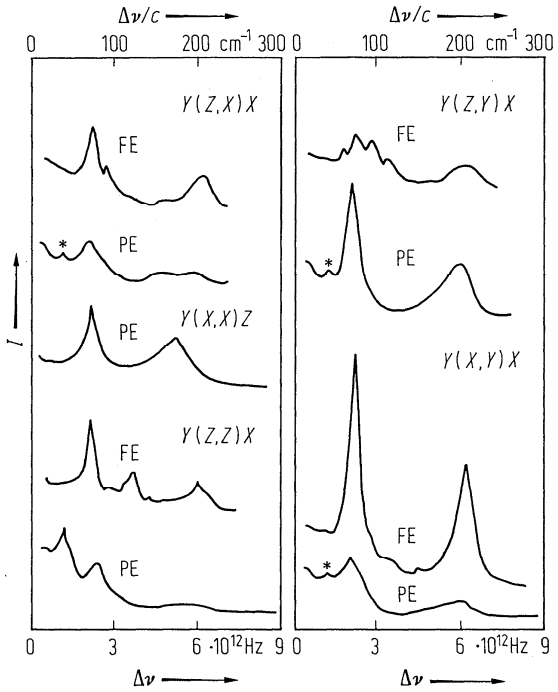

Fig. 39A-1-033. $(NH_4)_2SO_4$. I vs. $\Delta\nu$ [76Iqb]. I: Raman scattering intensity of the low frequency region in the paraelectric phase (PE) at 240 K and ferroelectric phase (FE) at 214 K. $\Delta\nu$: frequency shift of Raman scattering. Asterisks indicate spill-over of peaks of other symmetry.

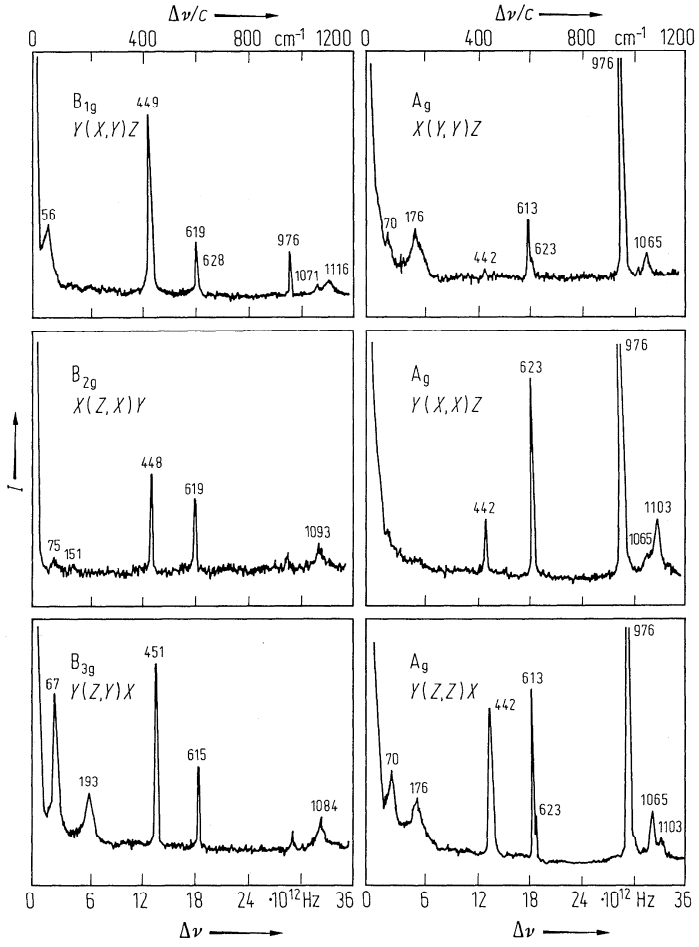

Fig. 39A-1-034. $(NH_4)_2SO_4$. I vs. $\Delta\nu$ [74Uch]. I: Raman scattering intensity at room temperature for various scattering geometries. $\Delta\nu$: frequency shift of Raman scattering. Peak frequencies are given in the figure in units of cm^{-1}.

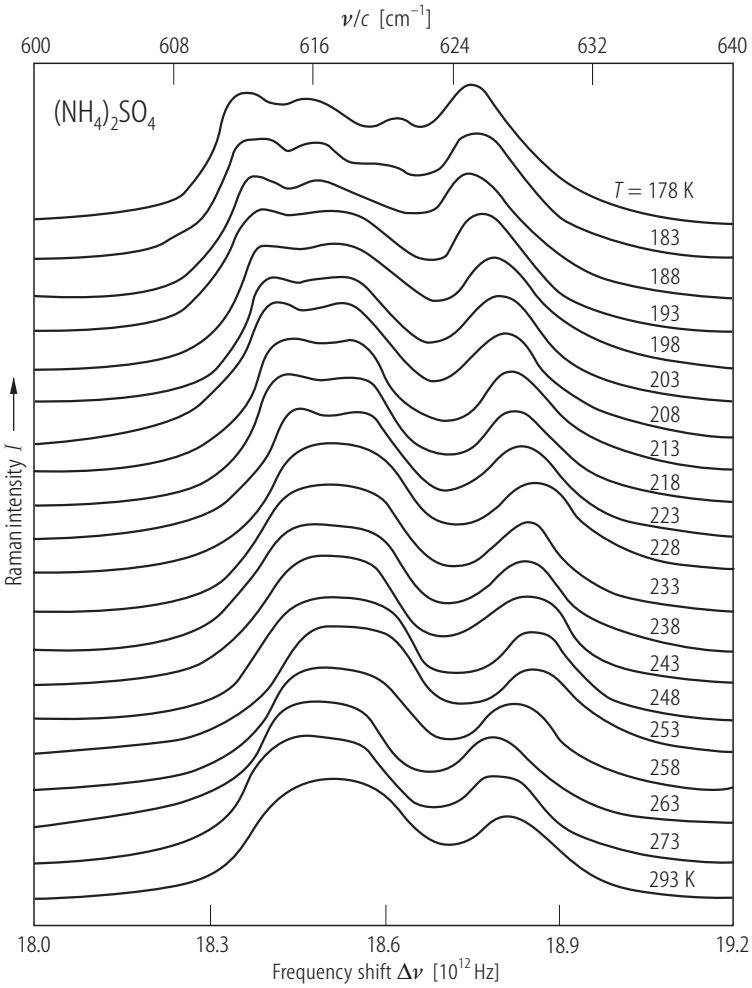

Fig. 39A-1-035. $(NH_4)_2SO_4$. I vs. $\Delta\nu$ [90Baj]. I: Raman scattering intensity of the ν_4 mode of the SO_4^{2-} ion. $\Delta\nu$: frequency shift of Raman scattering. Parameter: T.

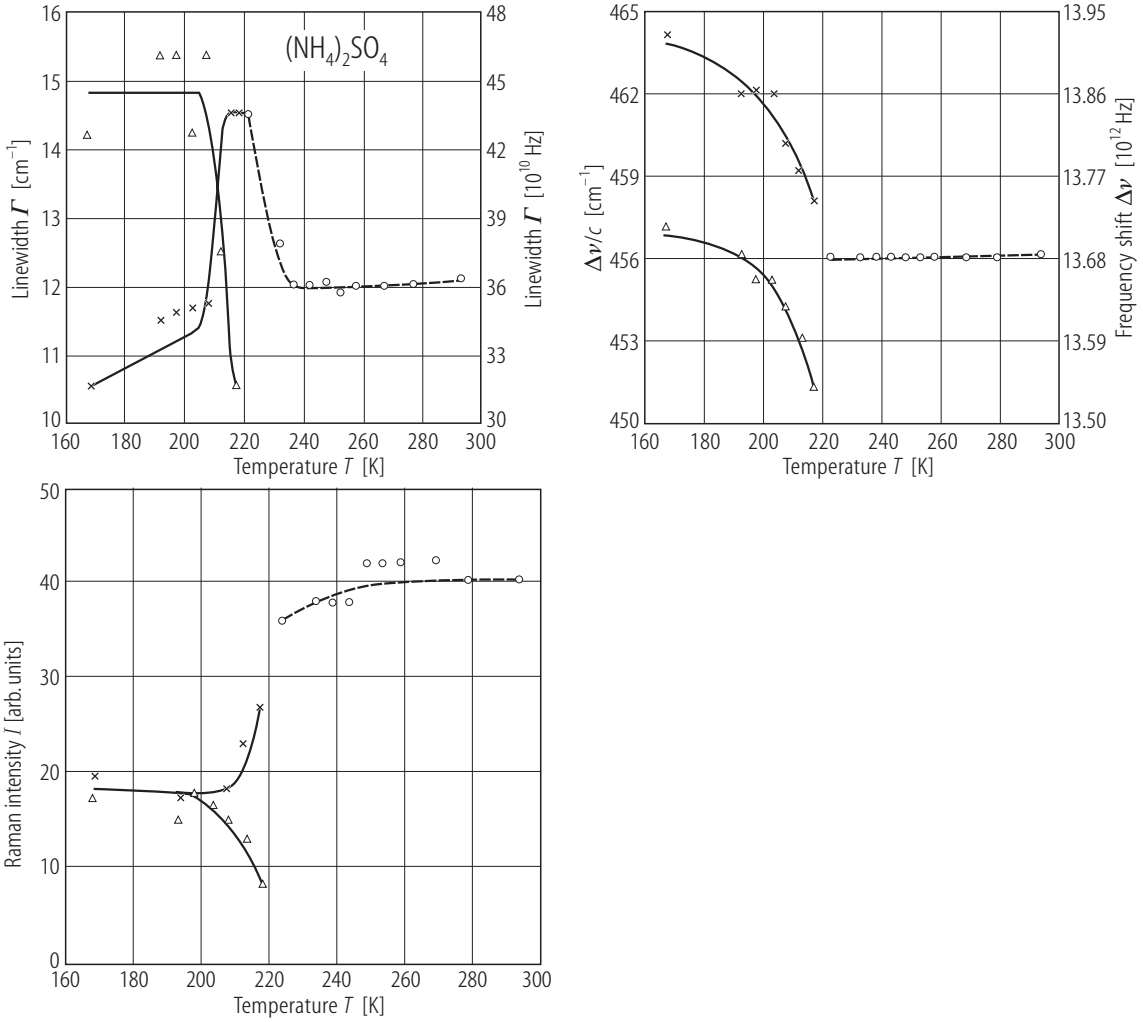

Fig. 39A-1-036. $(NH_4)_2SO_4$. Γ, $\Delta\nu$, I vs. T [90Baj]. The ν_2 mode of the SO_4^{2-} ion. Γ: Raman scattering linewidth, $\Delta\nu$: frequency shift of Raman scattering, I: Raman scattering intensity. The ν_2 mode splits into two branches (triangle and cross) below Θ.

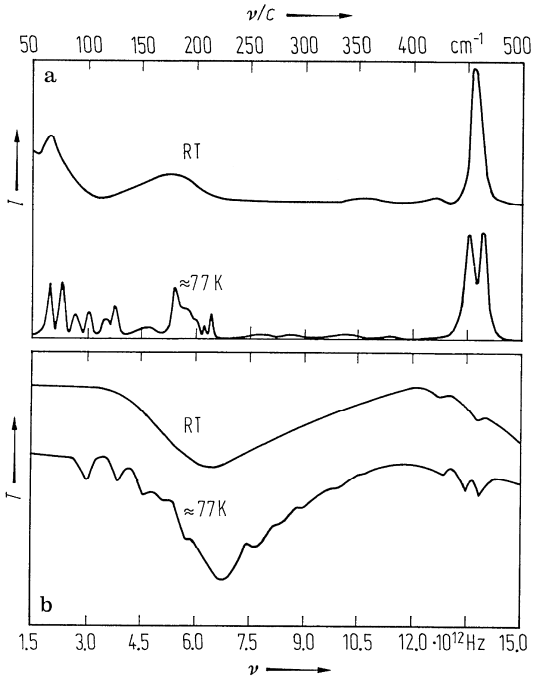

Fig. 39A-1-037. $(ND_4)_2SO_4$. I, T vs. ν [72Tor]. I: Raman scattering intensity (**a**), T: transmittance for the infrared radiation (**b**). Sample: polycrystal. ν: frequency shift in (**a**), and frequency of the incident radiation in (**b**).

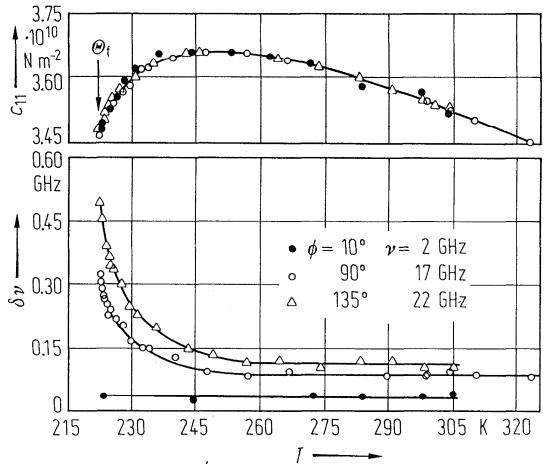

Fig. 39A-1-038. $(NH_4)_2SO_4$. c_{11}, $\delta\nu$ vs. T [78Unr]. c_{11}: elastic stiffness. $\delta\nu$: linewidth of phonon spectrum at different frequencies ν, i.e. different scattering angles ϕ.

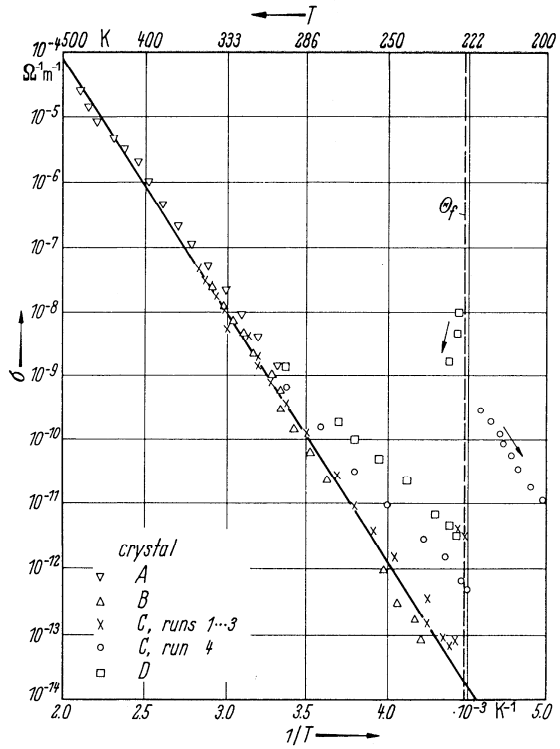

Fig. 39A-1-039. $(NH_4)_2SO_4$. σ vs. T^{-1} [63Sch]. All points near and below Θ_f were obtained from cooling runs, except for the three isolated high-conductivity points for crystal D which were obtained just above Θ_f while warming the crystal immediately after having cooled through the transition point. Conducting silver paint was applied on the (010) faces as electrodes: dc field of about 400 V was applied across crystals of 1…2 mm thickness. Probably the charge carriers are protons.

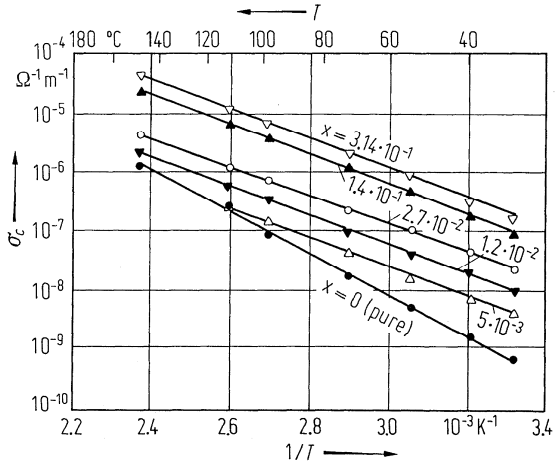

Fig. 39A-1-040. $(NH_4)_2SO_4$. σ_c vs. T^{-1} for $(HSO_4)^{-1}$ doped crystals [74Kha]. x: contents of $(HSO_4)^{-1}$ ions in $(NH_4)_2SO_4$ in mol%.

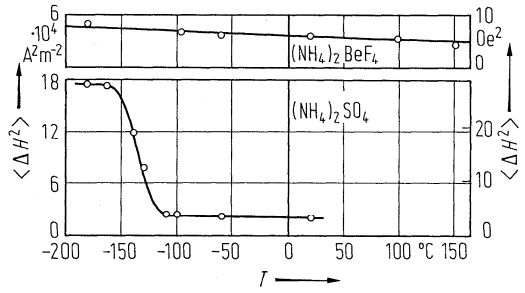

Fig. 39A-1-041. $(NH_4)_2SO_4$, $(NH_4)_2BeF_4$. $\langle \Delta H^2 \rangle$ vs. T [60Bli]. $\langle \Delta H^2 \rangle$: second moment of magnetic resonance curve of ^1H.

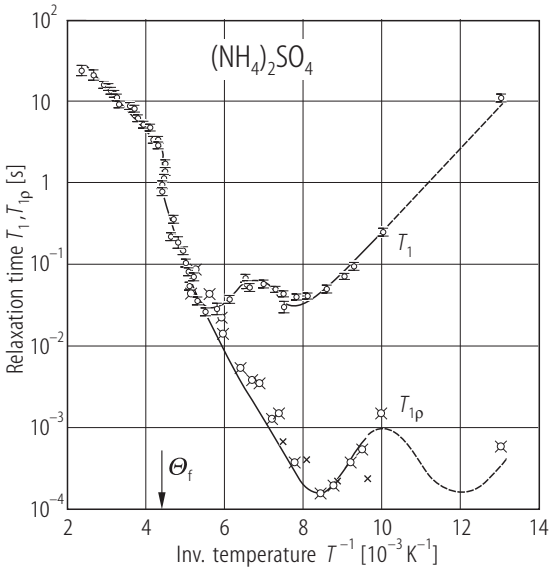

Fig. 39A-1-042. $(NH_4)_2SO_4$. T_1, $T_{1\rho}$ vs. T^{-1} [67ORe]. T_1: proton spin-lattice relaxation time; $T_{1\rho}$: proton spin-lattice relaxation time along the radio frequency field. Open circle: T_1 at 42 MHz; crossed circle: $T_{1\rho}$ by the method of Look et al. [66Loo]; cross: $T_{1\rho}$ by the method of Ostroff and Waugh [66Ost].

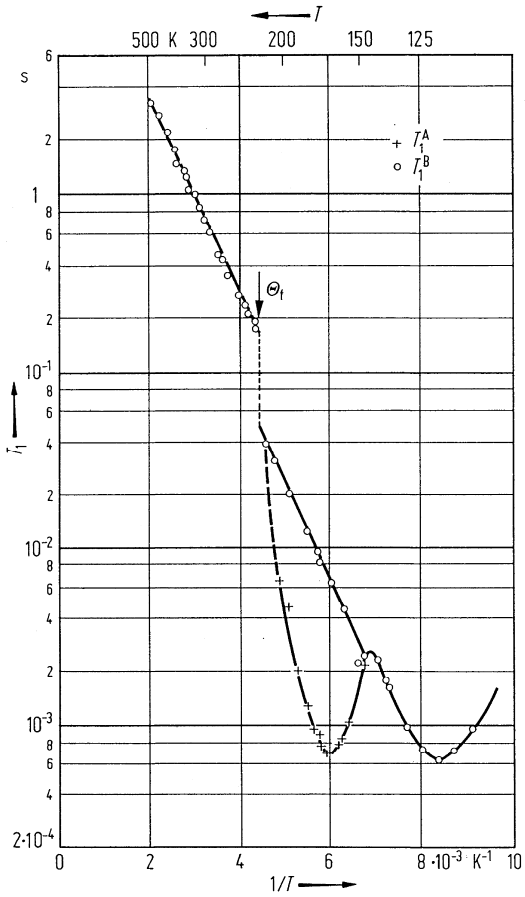

Fig. 39A-1-043. $(ND_4)_2SO_4$. T_1 vs. T^{-1} [69Kyd]. T_1: deuteron spin-lattice relaxation time. There are two well-separated sets of T_1 around Θ_f, denoted as T_1^A and T_1^B. $\nu_L = 11.5$ MHz.

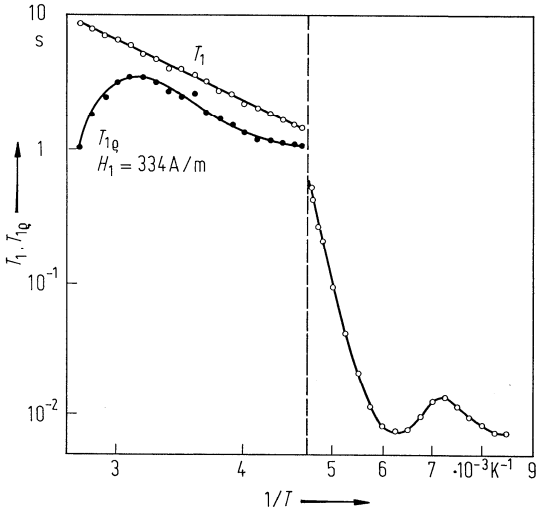

Fig. 39A-1-044. $(NH_4)_2SO_4$. T_1, $T_{1\rho}$ vs. $1/T$ [84Mor]. T_1 and $T_{1\rho}$ are spin-lattice relaxation times of proton in laboratory frame and rotating frame, respectively. $\nu_L = 16$ MHz. The scale of abscissa is changed at $1/T = 4.5 \cdot 10^{-3}$ K^{-1}.

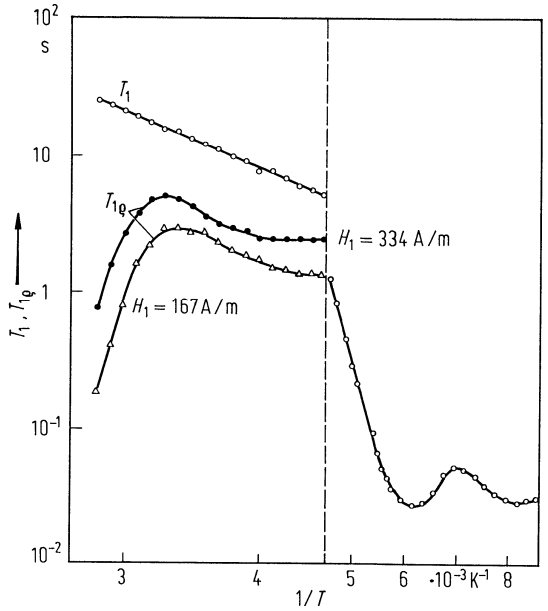

Fig. 39A-1-045. $(NH_{4(1-x)}D_{4x})_2SO_4$ (x = 0.75). T_1, $T_{1\rho}$ vs. $1/T$ [84Mor]. Parameter: H_1. T_1 and $T_{1\rho}$ are spin-lattice relaxation times of proton in laboratory frame and rotating frame, respectively. ν_L = 16 MHz. H_1: strength of rf field. The scale of abscissa is changed at $1/T = 4.5 \cdot 10^{-3}$ K^{-1}.

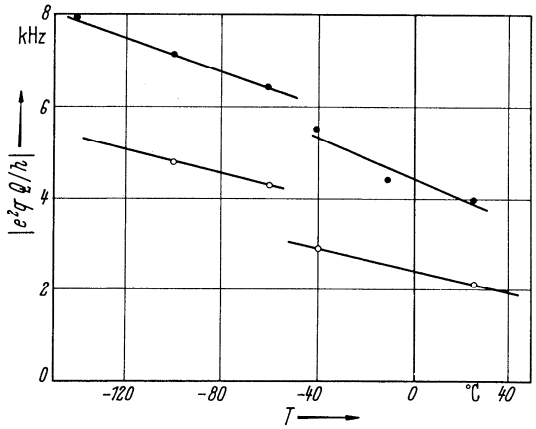

Fig. 39A-1-046. $(ND_4)_2SO_4$. $|e^2qQ/h|$ vs. T [67ORe]. $|e^2qQ/h|$: quadrupole coupling constant of ^{2}D. The different marks of data points correspond to the two inequivalent $(ND_4)^+$ ions.

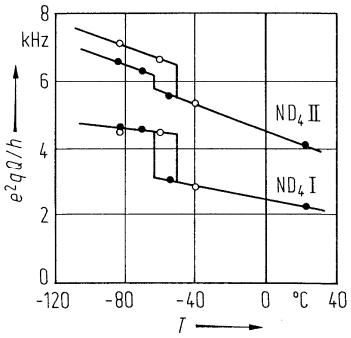

Fig. 39A-1-047. $(ND_4)_2SO_4$. e^2qQ/h vs. T [75Vin]. e^2qQ/h: quadrupole coupling constant of ^2D. ND_4 I and ND_4 II correspond to the two non-equivalent $(ND_4)^+$ ions. Open circles: at atmospheric pressure; full circles: under hydrostatic pressure of $3.5 \cdot 10^8$ Pa.

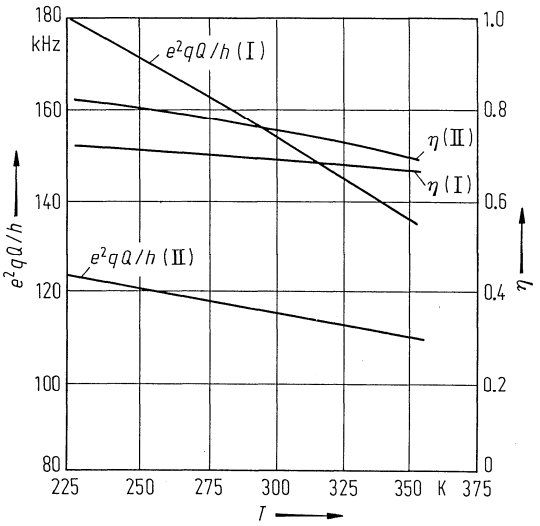

Fig. 39A-1-048. $(NH_4)_2SO_4$. e^2qQ/h, η vs. T for ^{14}N [80Bat]. I and II refer to different ^{14}N sites.

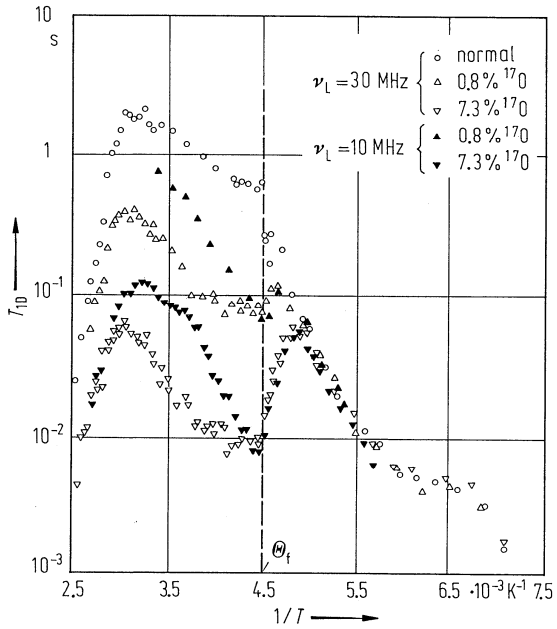

Fig. 39A-1-049. $(NH_4)_2SO_4$ (^{17}O enriched). T_{1D} vs. $1/T$ [85Chi]. T_{1D}: ^{17}O spin-lattice relaxation time in dipolar field.

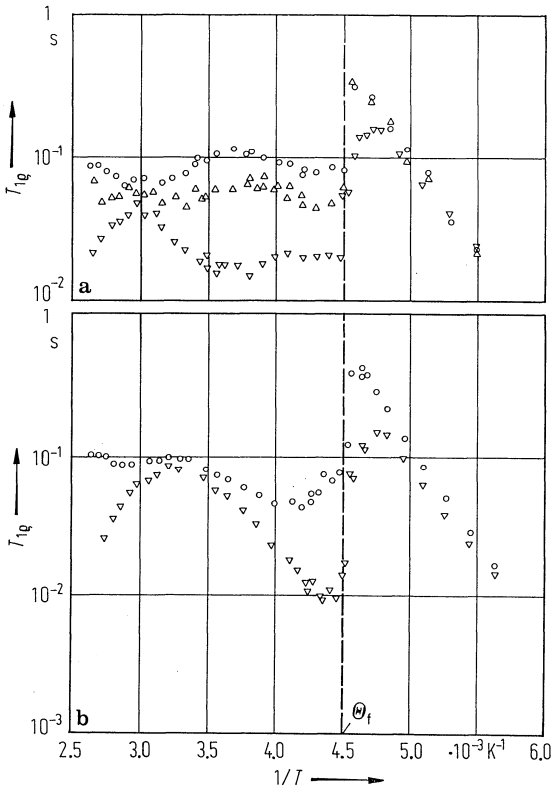

Fig. 39A-1-050. $(NH_4)_2SO_4$ (7.3% ^{17}O enriched). $T_{1\rho}$ vs. $1/T$ [85Chi]. Parameter: H_1. $T_{1\rho}$: ^{17}O spin-lattice relaxation time in rotating frame. (**a**) ν_L = 30 MHz; $H_1 = 1.4 \cdot 10^3$ A m^{-1} (circle), $1.0 \cdot 10^3$ A m^{-1} (upside triangle), $0.32 \cdot 10^3$ A m^{-1} (downside triangle). (**b**) ν_L = 10 MHz; $H_1 = 1.6 \cdot 10^3$ A m^{-1} (circle), $0.32 \cdot 10^3$ A m^{-1} (downside triangle).

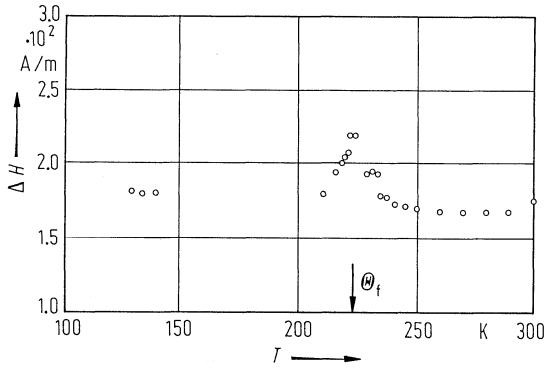

Fig. 39A-1-051. $(NH_4)_2SO_4$. ΔH vs. T [86Rav]. ESR. ΔH: linewidth for the high field singlet of the $(NH_3)^+$radicals. $f = 9.4$ GHz.

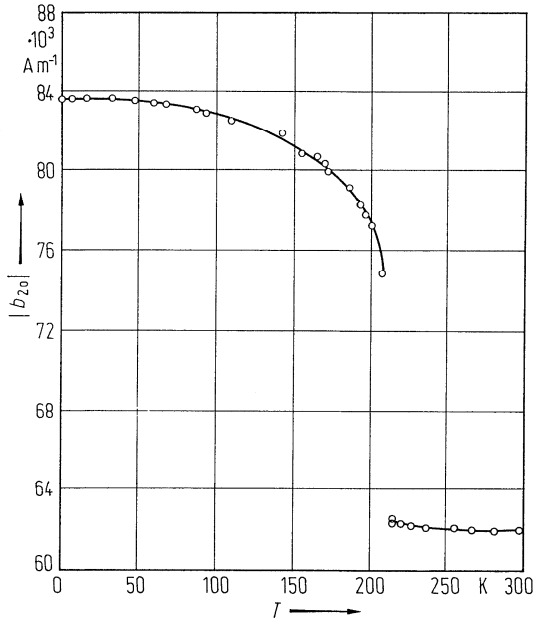

Fig. 39A-1-052. $(NH_4)_2SO_4$:Mn^{2+}. $|b_{20}|$ vs. T [72Adb]. ESR for Mn^{2+} doped crystal. b_{20}: FS parameter.

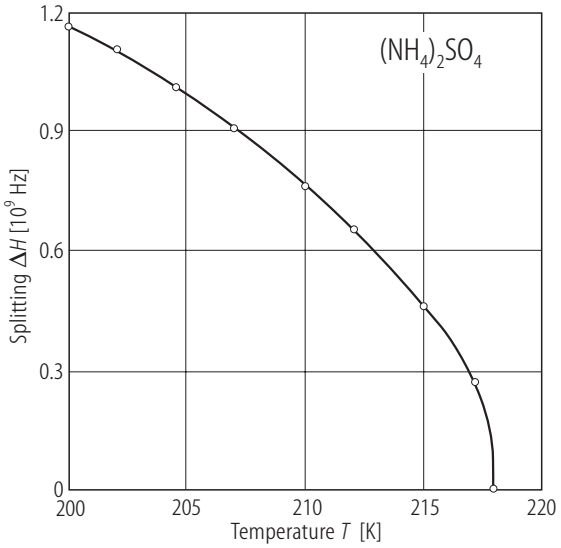

Fig. 39A-1-053. $(NH_4)_2SO_4$:Mn^{2+}. ΔH vs. T [88Mis]. ESR. ΔH: splitting of the (–3/2, 5/2 ↔ –5/2, 5/2) transition of Mn^{2+}. The continuous line indicates calculated values of $\Delta H = H_0[(\Theta - T)/\Theta]^{\beta}$ with H_0 = 4.053 GHz, Θ = 218 K, β = 0.5.

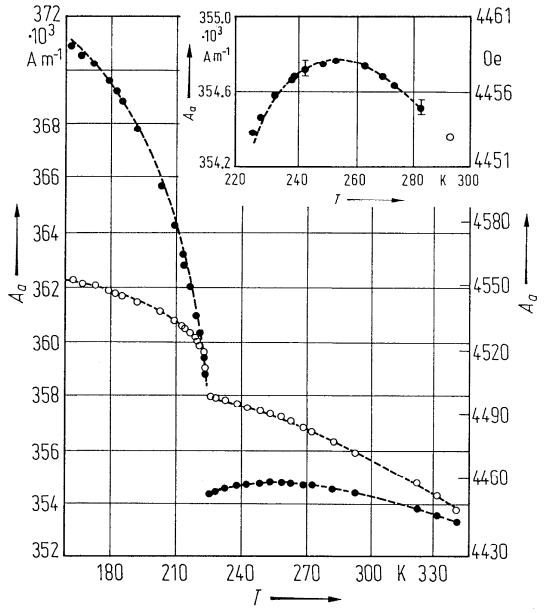

Fig. 39A-1-054. $(NH_4)_2SO_4$:Cd^+. A_a vs. T [78Bar]. ESR of Cd^+ impurity. A_a: hyperfine structure parameter of Cd^+. External magnetic field is parallel to the a axis, one of the principal axes of the $\boldsymbol{A}$ tensor. Full circles: Cd^+ in α-position; open circles: Cd^+ in β-position.

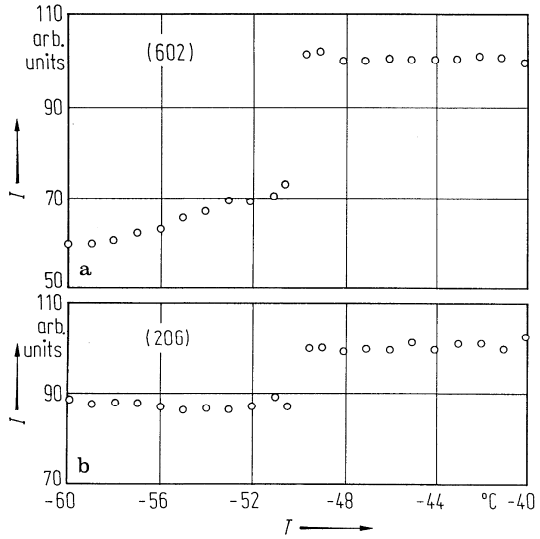

Fig. 39A-1-055. $(NH_4)_2SO_4$. (**a**) $I_{(6, 0, 2)}$, (**b**) $I_{(2, 0, 6)}$ vs. T [77Has]. I: integrated intensity of X-ray Bragg reflection.

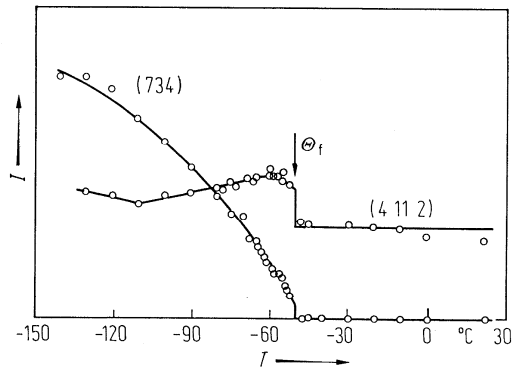

Fig. 39A-1-056. $(NH_4)_2SO_4$. $I_{(7, 3, 4)}$, $I_{(4, 11, 2)}$ vs. T [78Ono]. I: integrated intensity of X-ray Bragg reflection.